Biophysical Journal
Article

Biophysical Society

The Orphan Kinesin PAKRP2 Achieves Processive Motility via a Noncanonical Stepping Mechanism

Allison M. Gicking,[1] Pan Wang,[1,2] Chun Liu,[3] Keith J. Mickolajczyk,[4,5] Lijun Guo,[2] William O. Hancock,[4,5] and Weihong Qiu[1,6,*]

[1]Department of Physics, Oregon State University, Corvallis, Oregon; [2]School of Physics and Electronics, Henan University, Kaifeng, Henan, China; [3]Pearl River Fisheries Research Institute, Guangzhou, China; [4]Department of Biomedical Engineering and [5]Intercollege Graduate Degree Program in Bioengineering, Penn State University, University Park, Pennsylvania; and [6]Department of Biochemistry and Biophysics, Oregon State University, Corvallis, Oregon

ABSTRACT Phragmoplast-associated kinesin-related protein 2 (PAKRP2) is an orphan kinesin in *Arabidopsis thaliana* that is thought to transport vesicles along phragmoplast microtubules for cell plate formation. Here, using single-molecule fluorescence microscopy, we show that PAKRP2 is the first orphan kinesin to exhibit processive plus-end-directed motility on single microtubules as individual homodimers. Our results show that PAKRP2 processivity is achieved despite having an exceptionally long (32 residues) neck linker. Furthermore, using high-resolution nanoparticle tracking, we find that PAKRP2 steps via a hand-over-hand mechanism that includes frequent side steps, a prolonged diffusional search of the tethered head, and tight coupling of the ATP hydrolysis cycle to the forward-stepping cycle. Interestingly, truncating the PAKRP2 neck linker to 14 residues decreases the run length of PAKRP2; thus, the long neck linker enhances the processive behavior. Based on the canonical model of kinesin stepping, such a long neck linker is expected to decrease the processivity and disrupt the coupling of ATP hydrolysis to forward stepping. Therefore, we conclude that PAKRP2 employs a noncanonical strategy for processive motility, wherein a long neck linker is coupled with a slow ATP hydrolysis rate to allow for an extended diffusional search during each step without sacrificing processivity or efficiency.

INTRODUCTION

Kinesins constitute a diverse superfamily of ATP-dependent, microtubule-based motor proteins that are known to participate in a variety of intracellular processes, such as microtubule organization and dynamics (1–5) and the transport of cellular cargos (6,7). Previous studies have revealed that some kinesins are processive, meaning they take multiple consecutive steps along the microtubule before falling off, which allows them to transport organelles and protein complexes long distances (7–9). A specific example of cellular cargo transport occurs exclusively in plant cell division, which requires the construction of a cell plate at the division site. Plant kinesins hauling cell plate material walk on a microtubule-based structure called the phragmoplast, whose plus ends are located at the developing cell wall (10,11). In the model plant organism *Arabidopsis thaliana*, the phragmoplast-associated kinesin-related protein 2 (PAKRP2) is believed to transport Golgi vesicles to the phragmoplast midzone (12).

On the basis of phylogenetic analysis of the motor domains, the kinesin superfamily is divided into 14 subfamilies (kinesin-1 through kinesin-14) and an "orphan" (or ungrouped) family (13). PAKRP2 falls into the orphan family because of divergent structural features, such as a mutation in the conserved nucleotide-binding site (12,14). To date, no processive orphan kinesin has been reported, and many of the characterized orphan kinesins have mutations in the conserved residues essential for motility (15–19). Based on our current knowledge, PAKRP2's predicted function of long-distance vesicle transport is contradictory to its classification as an orphan kinesin, but no investigation of its motility has ever been done.

The ability to autonomously generate processive motility is not strictly required for kinesins to transport organelles (20), but it is a conserved feature of most transport kinesins, such as kinesin-1, kinesin-2, and kinesin-3 (21–23). In the canonical view, processive kinesins maintain tight coupling of the ATP hydrolysis cycle to the stepping cycle such that every ATP molecule leads to an 8.2-nm forward step

Submitted June 8, 2018, and accepted for publication February 19, 2019.

*Correspondence: weihong.qiu@physics.oregonstate.edu

Allison M. Gicking and Pan Wang contributed equally to this work.

Editor: Stefan Diez.

https://doi.org/10.1016/j.bpj.2019.02.019

(24,25). This coupling is achieved by an ATP-induced conformational change in the conserved 14–18 residue neck linker, which accelerates the trailing head to the next binding site before the lead head detaches (26–28). Currently, it is not known whether PAKRP2 is intrinsically processive or achieves transport of cargo via the clustering of several diffusive motors (20,29) or a nonmotor microtubule-binding domain that enhances the microtubule affinity of the motor domain via tethering (30,31).

In this study, we use a combination of single-molecule fluorescence microscopy, dark-field nanoparticle tracking, and solution ATPase assays to investigate the stepping mechanism of PAKRP2. We find PAKRP2 is a processive orphan kinesin that steps via a hand-over-hand mechanism that includes frequent lateral steps, a long-lived intermediate state, and tight coupling between ATP hydrolysis and forward stepping. Close examination of the PAKRP2 sequence revealed that it contains an unusually long (32 amino acid) neck linker that contributes to its processive behavior and does not adversely affect the coupling of the chemical ATPase activity to the mechanical stepping.

MATERIALS AND METHODS

Molecular cloning and protein expression and purification

The full-length complementary DNA of PAKRP2 was codon optimized for protein expression in *Escherichia coli* and synthesized as two gBlocks (Integrated DNA Technologies, Coralville, IA). The construct, containing a C-terminal His-tag, was integrated in a modified pET17b vector via isothermal assembly and verified by DNA sequencing. All of the truncation constructs were designed for this study except for K560AviC, which was created and characterized previously (32). For protein expression, plasmids were transformed into the BL21 Rosetta (DE3) competent cells (Novagen, Darmstadt, Germany). Cells were grown at 37°C in tryptone phosphate medium (containing 20 g tryptone, 15 g yeast extract, 8 g NaCl, 2 g Na_2HPO_4, and 1 g KH_2PO_4 per 1 L) supplemented with 50 μg/mL ampicillin and 30 μg/mL chloramphenicol. Expression was induced by a cold shock on ice at optical density $OD_{600} = 0.8–1$ with 0.1 mM isopropyl β-D-1-thiogalactopyranoside, and incubation was continued for an additional 14–17 h at 20°C. Cell pellets were harvested by centrifugation at 5500 × *g* for 10 min using a S-5.1 rotor (Beckman Coulter, Brea, CA) and stored at −80°C before cell lysis.

To purify the His-tagged PAKRP2 and kinesin-1 chimera motors, cell pellets were re-suspended in the lysis buffer (50 mM sodium phosphate buffer (pH 7.2), 250 mM NaCl, 1 mM $MgCl_2$, 0.5 mM ATP, 10 mM β-mercaptoethanol, 20 mM imidazole, 1 μg/mL leupeptin, 1 μg/mL pepstatin, 1 mM phenylmethylsulfonyl fluoride, and 5% glycerol) and lysed via sonication (Branson Sonifier 450; Branson Ultrasonics, Danbury, CT). The cell lysate was then centrifuged at 21,000 × *g* for 35 min using a Ti-75 rotor (Beckman Coulter). The supernatant was incubated with Talon beads (Clontech Laboratories, Mountain View, CA) by end-to-end mixing at 4°C for 1 h. The protein/beads slurry was then applied to a Poly-Prep column (Bio-Rad Laboratories, Hercules, CA) and washed twice with 10-column volumes of wash buffer (50 mM sodium phosphate buffer (pH 7.2), 250 mM NaCl, 1 mM $MgCl_2$, 0.1 mM ATP, 10 mM β-mercaptoethanol, 20 mM imidazole, 1 μg/mL leupeptin, 1 μg/mL pepstatin, 1 mM phenylmethylsulfonyl fluoride, and 5% glycerol). The protein was eluted with five-column volumes of elution buffer (50 mM sodium phosphate buffer (pH 7.2), 250 mM NaCl, 1 mM $MgCl_2$, 0.5 mM ATP, 10 mM β-mercaptoethanol, 250 mM imidazole, and 5% glycerol). The eluted protein was buffer exchanged with a PD-10 (desalting/buffer exchange column; GE Healthcare, Chicago, IL) column into storage buffer (BRB80, 0.5 mM ATP, 100 mM KCl, and 5% glycerol), flash frozen in liquid nitrogen, and stored at −80°C.

Polarity-marked microtubules

To make polarity-marked guanosine 5′-[(α,β)-methyleno]triphosphate (GMPCPP) microtubules, a dim bovine tubulin mix (containing 17 μM unlabeled tubulin, 17 μM biotinylated tubulin, and 0.8 μM HiLyte 647-tubulin) was first incubated in BRB80 with 0.5 mM GMPCPP (Jena Bioscience, Jena, Germany) at 37°C overnight to make dim microtubules and then centrifuged at 250,000 × *g* for 7 min at 37°C in a TLA100 rotor (Beckman Coulter). The pellet was resuspended in a bright bovine tubulin mix (containing 7.5 μM unlabeled tubulin, 4 μM HiLyte 647-tubulin, and 15 μM N-ethylmaleimide-tubulin) in BRB80 with 2 mM GMPCPP and incubated at 37°C for an additional 15 min to cap the plus end of the dim microtubules. The resulting polarity-marked track microtubules were pelleted at 20,000 × *g* for 7 min at 37°C in the TLA100 rotor (Beckman Coulter) and finally resuspended in BRB80 with 40 μM taxol.

Total internal reflection fluorescence microscopy

All time-lapse imaging assays were performed at room temperature (22–23°C) using the Axio Observer Z1 objective-type total internal reflection fluorescence microscope (ZEISS, Oberkochen, Germany) equipped with a 100× 1.46 numerical aperture oil-immersion objective and a back-thinned electron multiplier charge-coupled device camera (Photometrics, Huntington Beach, CA). All microscope coverslips were functionalized with biotin-polyethylene glycol as previously described (33) to reduce nonspecific surface absorption of molecules. All time-lapse imaging experiments in this study used flow chambers that were made by attaching a coverslip to a microscope glass slide by double-sided tape.

Single-molecule motility assay

For single-molecule motility experiments, the chamber was perfused with 0.5 mg/mL streptavidin to immobilize the taxol-stabilized polarity-marked HiLyte-647/biotin-labeled microtubules. After removing unbound microtubules by washing the chamber with five-chamber volumes of BRB12 supplemented with 20 μM taxol, the chamber was perfused with a BRB80-based (or BRB50 for Kin1_NLswap) motility mixture containing diluted motors, 1 mM ATP, 25 μM taxol, 1.3 mg/mL casein, and an oxygen scavenger system based on glucose oxidase/catalase (34). Time-lapse image sequences were recorded at one frame per 2 s with an exposure time of 200 ms for a duration of up to 10 min. Kymographs were generated and analyzed in ImageJ (National Institutes of Health, Bethesda, MD) for obtaining the velocity and run length information of individual PAKRP2 motors. Reported velocities are the peak of a Gaussian fit to the data, and associated errors are the SDs. Characteristic run lengths were calculated by fitting an exponential cumulative distribution function to the data and creating a bootstrap distribution to find the mean (n = 5000). The mean was then corrected for filament length using the procedure outlined in (35), in which the characteristic filament length is the average length of all microtubules used in the analysis. Reported errors are the 95% confidence intervals of the bootstrap distributions.

Single-molecule photobleaching assay

For single-molecule photobleaching assays, PAKRP2 molecules were immobilized, in the absence of ATP, on taxol-stabilized polarity-marked HiLyte-647/biotin-labeled microtubules in BRB80 with 20 μM taxol and 1.3 mg/mL casein. Time-lapse image sequences were continuously recorded with an exposure time of 100 ms until the field of view was

completely bleached of fluorescence signal. The number of photobleaching steps of individual PAKRP2 motors was obtained by tracking the fluorescence intensity in ImageJ (National Institutes of Health). Photobleaching assays and single-molecule motility assays were performed at identical motor concentrations of 30–40 pM.

Total internal reflection dark-field microscopy assays

For single-molecule tracking experiments, we used a custom-built total internal reflection dark-field microscope as previously described (36). All experiments were carried out at 22–23°C. PAKRP2 motors were prepared with a biotinylated C-terminal Avi-tag or biotinylated green fluorescent protein binding protein (37) and mixed with a 30-nm diameter, streptavidin-coated gold nanoparticles. The motor was added to the gold particles at the lowest molar ratio that produced landing events (4:1 for PAKRP2 and 3:1 for K560AviC). Taxol-stabilized guanine diphosphate (GDP) microtubules were attached to the glass coverslip via a kinesin rigor mutant as previously described (32). High-resolution position versus time traces were obtained from 100 frame/s (or 1000 frame/s for kinesin-1) videos by fitting the point-spread function with a two-dimensional Gaussian using Fiesta software (38). The x and y trajectories were rotated to minimize the SD in the x direction, resulting in a y axis that is aligned with the microtubule axis.

Step size determination

The on-axis step sizes were determined by a t-test algorithm (39) for the y displacement versus time traces. Only the traces with an SD of <3 nm from the step plateau were chosen for analysis. All reported step sizes are the mean $\pm$ SD of a single Gaussian fit to the forward steps.

ATPase assay

ATPase assays were carried out by an enzyme-coupled assay protocol adapted from a previous study (40). Assays used 25 nM active dimeric PAKRP2(560) and 5 nM active dimeric Kin1_NLswap, in which activity was determined by assessing exchange of 3'-O-(N-methylanthraniloyl)adenosine 5'-diphosphate, as previously described (41). Hydrolysis rates at each microtubule concentration (GDP taxol-stabilized) were estimated by a linear fit to steady-state absorbance decreases at 340 nm, as previously described (41). The k_{cat} and K_M were determined by performing a least-squares fit of the ATPase versus tubulin concentration curve to the Michaelis-Menten equation.

RESULTS

PAKRP2 is a processive orphan kinesin with a long neck linker

PAKRP2 consists of an N-terminal motor domain followed by a neck linker, a coiled-coil central stalk, and an uncharacterized C-terminal tail. Based on previous studies that show that the neck linker is an important component of kinesin processivity (22,42–45) and the fact that PAKRP2 is an orphan kinesin (12,14,46), we first wanted to determine whether PAKRP2 contains any structural divergences in the neck linker region. Two coiled-coil prediction programs, COILs (47) and MARCOIL (48), both place the likely start of the α-7 helix between residues 394 and 407 (Fig. 1, *A* and *B*). Examination of the sequence within that range places the first logical heptad repeat of the coiled-coil domain at residue 397, a hydrophobic methionine, followed by negatively charged aspartic and glutamic acids (Fig. 1 *C*). Thus, we concluded that the neck linker of PAKRP2 contains 32 residues, considerably longer than the neck linkers of other kinesins, which typically contain 14–18 residues (26).

Several studies on kinesin-1 and kinesin-2 demonstrate that increasing the neck linker length can lead to disruptions

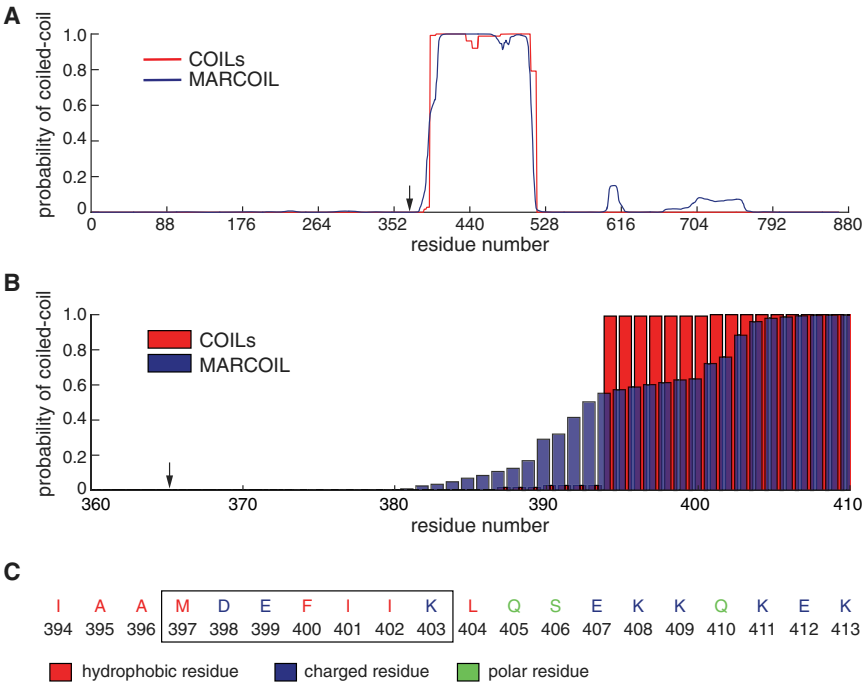

FIGURE 1 PAKRP2 contains a long neck linker. (*A*) The coiled-coil profiles of full-length PAKRP2 predicted by COILs (*red*) and MARCOIL (*blue*) are shown. Black arrow denotes the end of the motor domain. (*B*) Shown are the zoomed-in coiled-coil profiles of residues just before the coiled-coil region. Black arrow denotes the end of the motor domain. (*C*) Shown is the sequence of residues between 394 and 413 to show first heptad repeat starting at residue 397 and ending at residue 403. To see this figure in color, go online.

in the stepping mechanism, such as a decrease in run length or an increase in futile ATP hydrolysis cycles (43,49–51). To determine whether PAKRP2 is a processive microtubule motor, we engineered a recombinant full-length PAKRP2 with a C-terminal green fluorescent protein (PAKRP2(FL)) (Fig. 2, *A* and *B*). We used a single-molecule motility assay to visualize the movement of PAKRP2(FL) on polarity-marked microtubules (Fig. 2, *C* and *D*; Videos S1 and S2). The assay showed that individual PAKRP2(FL) molecules moved processively toward microtubule plus ends with a mean velocity of 65 ± 16 nm s^{-1} (mean ± SD, n = 271; Fig. 2 *E*) and a run length of 3.6 ± 0.3 μm (mean ± 95% confidence intervals, n = 271, Fig. 2 *F*). The reported run lengths and the associated error are the mean and 95% confidence intervals of the bootstrap distribution. It is well established that nonprocessive kinesin motors can achieve

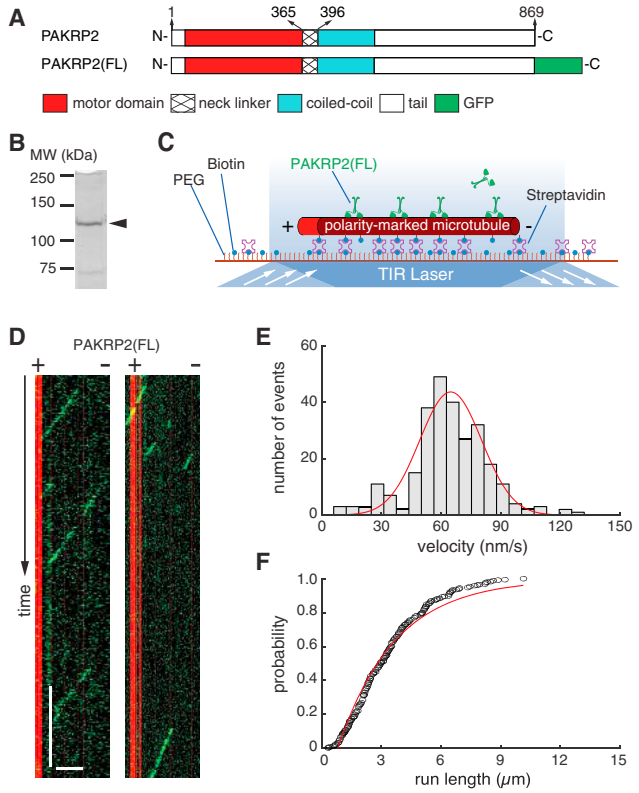

FIGURE 2 Full-length PAKRP2 is a processive plus-end-directed kinesin. (*A*) Shown are schematic diagrams of full-length PAKRP2 and PAKRP2(FL). (*B*) Sodium dodecyl sulfate polyacrylamide gel electrophoresis of PAKRP2(FL) is shown. Arrowhead indicates the expected band of PAKRP2(FL); molecular weight = 126 kDa. (*C*) Schematic diagram of the single-molecule motility assay is shown. (*D*) Shown are representative kymographs of individual PAKRP2(FL) molecules moving processively toward the plus ends of single microtubules. Scale bars, 2 min (*vertical*), 5 μm (*horizontal*). (*E*) Velocity histogram of PAKRP2(FL) is shown. Red line corresponds to a Gaussian fit with a mean value of 65 ± 16 nm s^{-1} (n = 271). (*F*) The cumulative distribution of PAKRP2(FL) run length has a characteristic run length of 3.6 ± 0.3 μm (n = 271). Black circles correspond to experimental data, and the red line corresponds to an exponential cumulative distribution function fit. To see this figure in color, go online.

processive motility by clustering to form multimotor ensembles (20,29). We thus performed single-molecule photobleaching to determine the oligomerization of PAKRP2(FL). Similar to other dimeric kinesins (20), PAKRP2(FL) was predominantly photobleached in one or two steps (Fig. S1, *A* and *B*). These results show that PAKRP2(FL) contains the ability to exhibit processive plus-end-directed motility on single microtubules as a homodimer.

Some kinesins are known to achieve processive motility or to gain enhanced processivity via nonmotor microtubule-binding domains (30,31,52). To test whether PAKRP2 processivity depends on any domain beyond the head and neck linker domains, we made two additional constructs: a PAKRP2 truncation containing residues 1–560 (PAKRP2(560)) and an artificial dimer of PAKRP2 containing residues 1–403 and dimerized through a leucine zipper (PAKRP2(LZ)) (Fig. 3, *A–C*). Single-molecule photobleaching experiments confirmed that PAKRP2(560) and PAKRP2(LZ) both exist predominantly as individual homodimers (Fig. S1, *C–F*) and exhibited processive plus-end-directed motility on single microtubules (Fig. 3 *D*; Videos S3 and S4). The velocities of PAKRP2(560) and PAKRP2(LZ) were within 7% of the PAKRP2(FL) velocity (Fig. 3 *E*; Fig. S2, *A* and *C*). Run lengths of PAKRP2(560) and PAKRP2(LZ) were determined to be 3.4 ± 0.3 μm (n = 266, Fig. 3 *E*; Fig. S2 *B*) and 2.7 ± 0.3 μm (n = 333, Fig. 3 *E*; Fig. S2 *D*), respectively. Although the PAKRP2(560) run length was within 6% of the PAKRP2(FL) run length, the decrease in run length of the PAKRP2(LZ) construct likely indicates that the native coiled coils play a role in motility. Overall, these data show that PAKRP2 processivity is largely encoded in the region containing the motor domain and the neck linker.

PAKRP2 frequently moves laterally

Based on the knowledge that PAKRP2 is inherently processive despite having a long neck linker, we next investigated its stepping behavior to determine whether and how it may differ from that of kinesin-1. We attached a 30-nm gold particle to the C-terminus of PAKRP2(560) and observed the center-of-mass motion via dark-field nanoparticle tracking (Fig. 4 *A*) (27). Gold nanoparticle attachment did not substantially affect the motor activity as the single-molecule velocity of nanoparticle-labeled motors on taxol-stabilized GDP microtubules was within 20% of the motors without nanoparticles in the same experimental conditions (Fig. S3). It should also be noted that the velocity of PAKRP2(560) without a conjugated gold nanoparticle on GDP microtubules was 36% slower than its velocity without a conjugated gold nanoparticle on GMPCPP microtubules (Fig. S3). One possible explanation might be that PAKRP2(560) is sensitive to the structural changes of the microtubule lattice because of the different nucleotide states

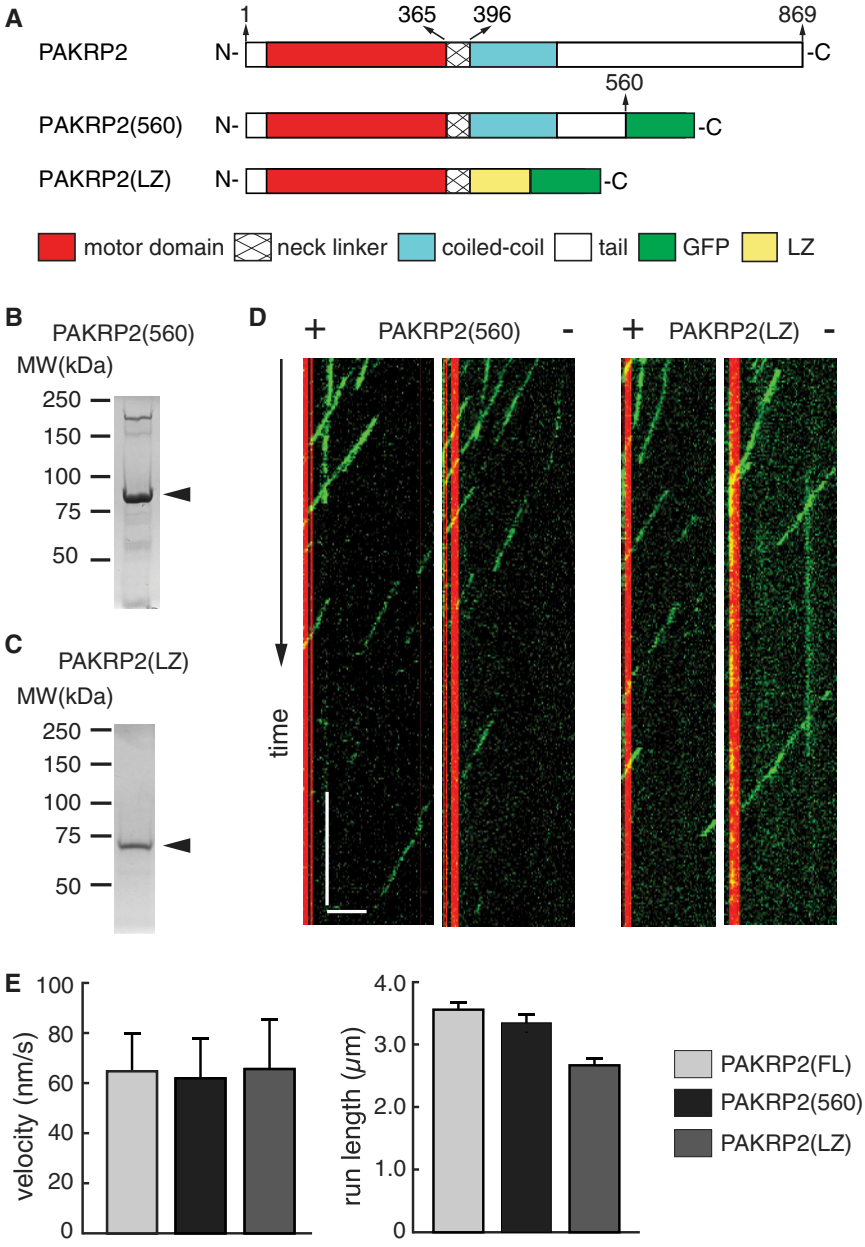

FIGURE 3 PAKRP2 processivity does not require a C-terminal tail or stalk domain. (*A*) Shown is a schematic diagram of full-length PAKRP2, PAKRP2(560), and PAKRP2(LZ). (*B*) Shown is sodium dodecyl sulfate polyacrylamide gel electrophoresis for PAKRP2(560). Arrowhead indicates the expected band of PAKRP2(560). Molecular weight = 91 kDa. (*C*) Shown is sodium dodecyl sulfate polyacrylamide gel electrophoresis for PAKRP2(LZ). Arrowhead indicates the expected band of PAKRP2(LZ). Molecular weight = 76 kDa. (*D*) Shown are representative kymographs of individual PAKRP2(560) and PAKRP2(LZ) molecules on single microtubules. Scale bars, 2 min (*vertical*), 5 μm (*horizontal*). (*E*) Bar graphs showing the relative velocities and run lengths of PAKRP2(FL), PAKRP2(560), and PAKRP2(LZ) with corresponding errors; SD for the velocity values and 95% confidence interval of the bootstrap distribution for the run length values. To see this figure in color, go online.

(53), which has also been observed in the motility of kinesin-1 (54,55).

When imaged at high resolution, PAKRP2(560) appeared to take frequent lateral steps both to the left and right (Fig. 4 *B*). To rule out that this behavior was due to the surface binding of the gold nanoparticle or some other artifact of the assay, we used kinesin-1 with a gold nanoparticle on the C-terminus as a control (K560AviC, Fig. 4 *C*) because kinesin-1 has been demonstrated to preferentially walk on single protofilaments unless it encounters a roadblock (56,57). The different lateral stepping characteristics of PAKRP2(560) with a gold nanoparticle on the C-terminus can be seen clearly when compared to K560AviC (Fig. 4 *D*).

To quantify the lateral stepping behavior, a distribution of the lateral displacement per 40 nm of on-axis displacement was generated for both motors (Fig. 4 *E*). The SDs for the Gaussian fits to the histograms of average off-axis displacements were 12.3 nm (n = 99) and 5.1 nm (n = 113) for PAKRP2 and kinesin-1, respectively, confirming that PAKRP2 steps laterally more than kinesin-1.

Canonical processive kinesins are known to take sequential 8-nm center-of-mass steps for the duration of their run lengths, matching the periodicity of tubulin binding sites on a single protofilament (58–60). Using point-spread-function fitting to the gold nanoparticle position and a *t*-test step-finding algorithm (Fig. 4 *F*), we measured an on-axis,

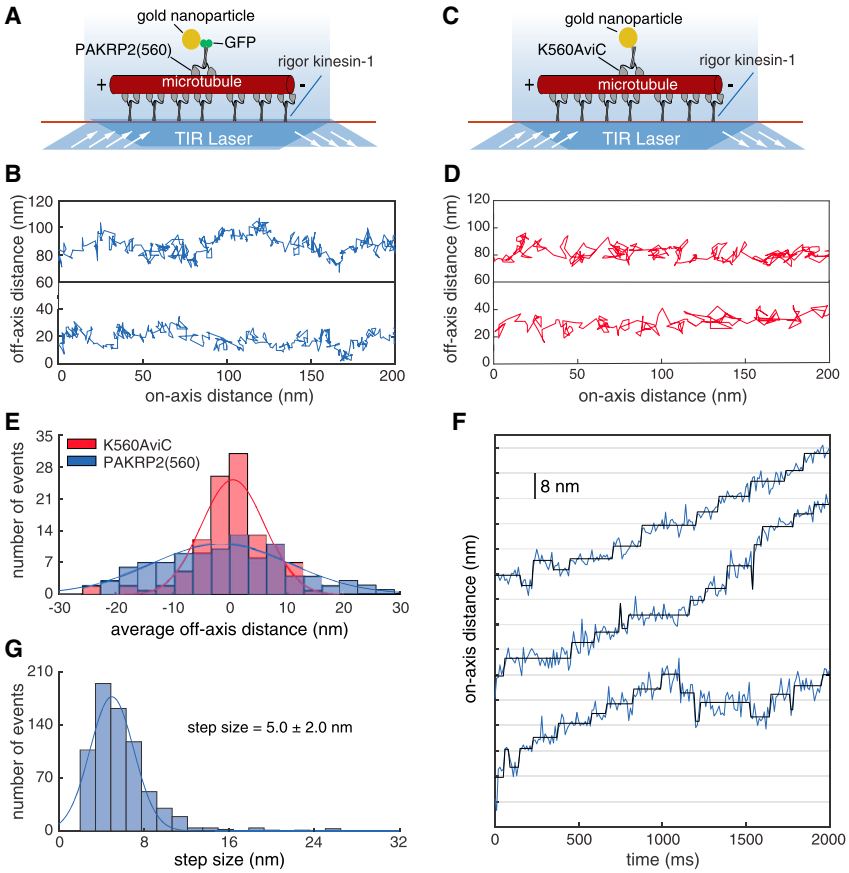

FIGURE 4 PAKRP2 takes frequent lateral steps. (*A*) Shown is a schematic diagram of the gold nanoparticle placement on the C-terminus of PAKRP2(560). (*B*) Shown are sample traces for PAKRP2(560), in which the horizontal axis corresponds to the microtubule axis, and the vertical axis corresponds to lateral movement. (*C*) Shown is a schematic diagram of the gold nanoparticle placement on the C-terminus of K560AviC. (*D*) Shown are sample traces for K560AviC, in which the horizontal axis corresponds to the microtubule axis, and the vertical axis corresponds to lateral movement. (*E*) Off-axis distance distributions for PAKRP2(560) and K560AviC are shown. Red and blue lines correspond to a Gaussian fit to the data. (*F*) A representative on-axis distance versus time plot is shown. Raw data are shown as blue lines, and steps detected by the *t*-test step-finding algorithm are shown in black. Data was acquired at 1 mM ATP every 10 ms. (*G*) Step-size histogram of PAKRP2(560) was fitted to a single Gaussian; n = 958. To see this figure in color, go online.

center-of-mass step size of 5.0 ± 2.0 nm for PAKRP2(560) (mean ± SD, n = 958, Fig. 4 *G*). In comparison, the kinesin-1 control displayed an on-axis, center-of-mass step size of 8.0 ± 3.0 nm (mean ± SD, $n = 664$, Fig. S4, *A* and *B*), consistent with previous results (59,61). Thus, PAKRP2 stepping is distinct from that of kinesin-1 in both the lateral movement and the average step size.

PAKRP2 takes intermediate steps

To better understand the individual head dynamics during PAKRP2 stepping and to confirm the small step size seen in the center-of-mass data, we attached the gold nanoparticle to one motor domain (head) of PAKRP2(560) via an N-terminal Avi-tag (Fig. 5 *A*). Similar to the center-of-mass construct, the head-tagged motor stepped processively along the microtubule with clearly observable steps (Fig. 5 *B*). Using the *t*-test step-finding algorithm, we measured an average step size of 7.6 ± 3.4 nm (mean ± SD, n = 230, Fig. 5 *C*). This value is larger than the center-of-mass step size but is only half of the 16.4 nm expected for a canonical hand-over-hand stepper (49,62). There are two plausible explanations for observing a step size smaller than the distance between successive binding sites on a single protofilament: 1) the labeled head is binding to an adjacent protofilament in an inchworm-like stepping mechanism (63,64) or 2) the step represents a transient intermediate in which the labeled head is transiting between successive binding sites. For instance, Stepp et al. (65) demonstrated that head-labeled kinesin-2 motors take 13-nm steps on single microtubules compared with 16-nm steps on axonemes. This discrepancy was explained by 50% of the steps landing on an adjacent site 8.2 nm away on microtubules. In contrast, high-resolution nanoparticle tracking of kinesin-1 labeled on only one head revealed a transient intermediate in the 16.2-nm step that resulted in an average measured step size of 8.2 nm (32).

To resolve whether the PAKRP2 motor domains are taking 8.2-nm steps to adjacent protofilaments or pausing midway through 16.4-nm steps, we measured the ATPase activity of PAKRP2. Canonical steppers are tightly coupled, meaning their center-of-mass takes one 8.2-nm forward step for every ATP molecule hydrolyzed (24,66). It is important to remember here that the displacement of the motor's center-of-mass is approximately half the displacement of one motor head if the second head remains bound to the microtubule. Based on the measured velocity of 40 ± 12 nm s^{-1} on GDP taxol-stabilized microtubules (Fig. S3), 8.2-nm steps of the center-of-mass correspond to a stepping rate of 4.9 s^{-1}, and 4.1-nm steps correspond to a stepping rate

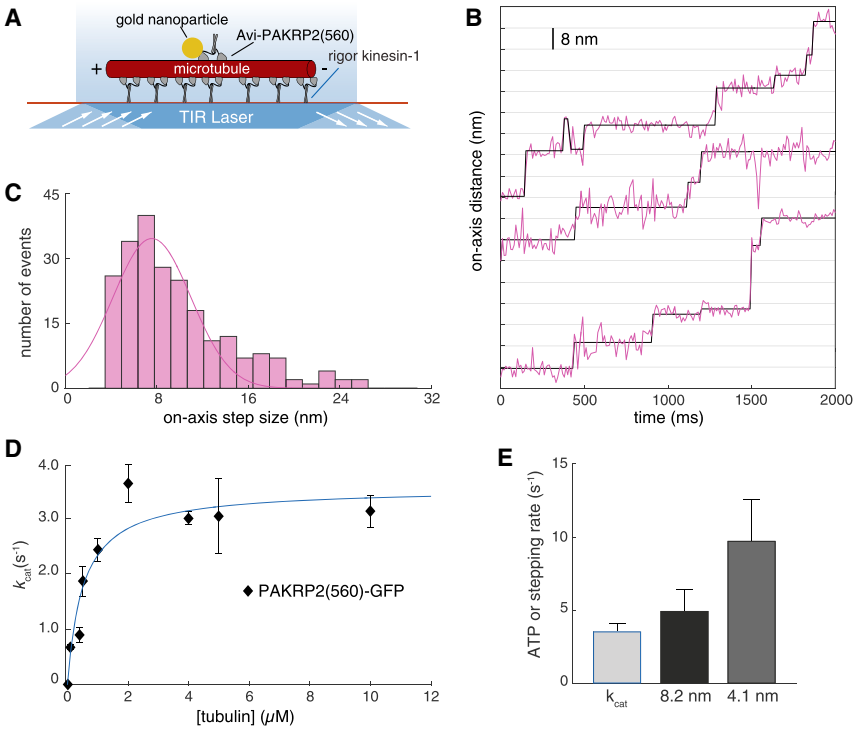

FIGURE 5 PAKRP2 takes intermediate steps. (*A*) Shown is a schematic diagram of the gold nanoparticle placement on the N-terminal motor domain of Avi-PAKRP2(560). (*B*) A representative on-axis distance versus time plot is shown. Raw data are shown as purple lines, and steps detected by the *t*-test step-finding algorithm are shown in black. Data were acquired at 1 mM ATP every 10 ms. (*C*) Step size histogram of Avi-PAKRP2(560) was fit to a single Gaussian; n = 230. (*D*) The ATPase rate per dimer for PAKRP2(560) as a function of tubulin concentration is shown. Data correspond to the mean ± standard error (n = 3 or 5 determinations per point). The solid line represents a fit to the Michaelis-Menten equation, giving a maximal k_{cat} of 3.5 ± 0.6 s^{-1}. (*E*) Comparison of the ATP hydrolysis rate per dimer and the stepping rate per dimer assuming different step sizes, is shown. Stepping rates were calculated from the division of the center-of-mass mean velocity by the center-of-mass step size. To see this figure in color, go online.

of 9.8 s^{-1}. In the ATPase assay, the k_{cat} for a PAKRP2(560) dimer was 3.5 ± 0.6 ATP/s (Fig. 5 *D*), which is consistent with the rate for 8.2-nm center-of-mass steps (Fig. 5 *E*). Therefore, we conclude that PAKRP2 stepping includes a long-lived intermediate state, with the final position of the head being ~16.4 nm from the starting position. This result also necessitates that PAKRP2 hydrolyzes one ATP per 8.2-nm step, despite having a long neck linker, which is contrary to previous studies on kinesin-1 in which long neck linkers lead to uncoupling of the ATPase activity from stepping (49,51).

PAKRP2 neck linker disrupts kinesin-1 stepping

The finding that PAKRP2 contains a long neck linker yet retains tight coupling between its ATPase and stepping activities raises the possibility that sequence-specific structural features in its long neck linker contribute to the coupling. To test whether the PAKRP2 neck linker confers tight coupling to other motors, we designed a kinesin-1 chimera, Kin1_NLswap, in which the native 14-residue neck linker was replaced by the 32-residue neck linker from PAKRP2 (Figs. 6 *A* and S5 *A*). A single-molecule photobleaching assay confirmed that this construct is a homodimer in solution (Fig. S5, *B* and *C*). From kymograph analysis (Video S5), the single-molecule velocity of Kin1_NLswap was 103 ± 20 nm s^{-1} (n = 172, Fig. 6 *B*), and the run length was 1.6 ± 0.2 μm (n = 172, Fig. 6 *C*). Under similar conditions, the velocity and run length of wild-type kinesin-1 are 670 ± 70 nm s^{-1} and 1.2 ± 0.2 μm, respectively (27). Thus, swapping the PAKRP2 neck linker into kinesin-1 decreases the velocity but does not adversely alter motor processivity.

In principle, this slower velocity could result from either the slowing of the ATPase cycle or uncoupling of the hydrolysis cycle from the stepping cycle such that ATP hydrolysis does not always lead to a forward step. To test between these possible mechanisms, we measured the microtubule-stimulated ATPase of Kin1_NLswap. The k_{cat} of the Kin1_NLswap was 121 ± 7 s^{-1} (Fig. S6), which is 10-fold higher than the center-of-mass stepping rate of ~12 s^{-1}, assuming it takes 8.2-nm hand-over-hand steps. However, even if the steps were 4.1-nm inchworm steps, the stepping rate of ~25 s^{-1} would still be considerably lower than the ATP hydrolysis rate. Thus, replacing the kinesin-1 neck linker with the longer PAKRP2 neck linker led to the uncoupling of the kinesin-1 from its forward stepping activity. It follows that the tight coupling mechanism in PAKRP2 requires features in the catalytic domain of the motor and is not exclusively due to specific structural features of the neck linker.

PAKRP2 neck linker enhances its processivity

Given that the neck linker from PAKRP2 greatly disrupts the stepping cycle of kinesin-1, it could also negatively impact the stepping cycle of PAKRP2. To determine the role of the extended neck linker in the processivity of PAKRP2, we

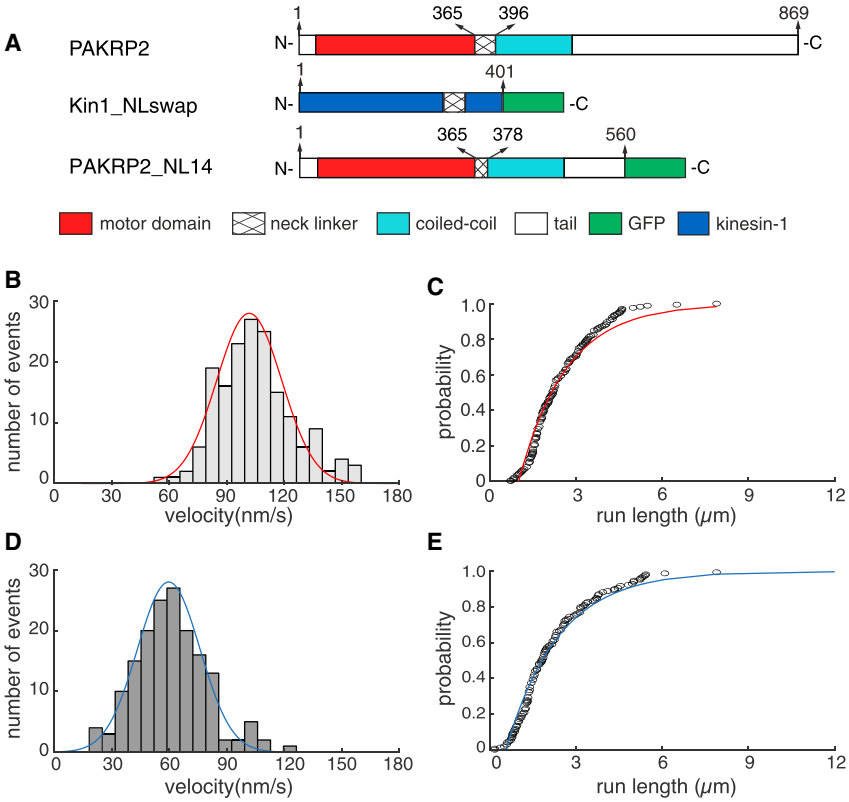

FIGURE 6 PAKRP2 neck linker affects processivity. (*A*) Shown is a schematic diagram of Kin1_NLswap and PAKRP2_NL14. (*B*) Velocity histogram of Kin1_NLswap is shown. Red line corresponds to a Gaussian fit with a mean of 103 ± 20 nm s^{-1} (n = 172). (*C*) Shown is the cumulative distribution of Kin1_NLswap with a characteristic run length of 1.6 ± 0.2 μm (n = 172). Black circles correspond to experimental data, and the red line corresponds to an exponential cumulative distribution function fit. (*D*) Velocity histogram of PAKRP2_NL14 is shown. Blue line corresponds to a Gaussian fit with a mean of 59 ± 19 nm s^{-1} (n = 168). (*E*) Shown is the cumulative distribution of the PAKRP2_NL14 run length. Black circles correspond to experimental data, and the blue line corresponds to an exponential cumulative distribution function fit with a characteristic run length of 2.0 ± 0.3 μm (n = 168). To see this figure in color, go online.

made a mutant, PAKRP2_NL14, in which neck linker residues beyond the first 14 amino acids in the sequence were deleted (Figs. 6 *A* and S5 *D*). The construct was also confirmed to be a homodimer (Fig. S5, *E* and *F*). In contrast to the change in velocity resulting from swapping the neck linker into kinesin-1, shortening the PAKRP2 neck linker did not affect the stepping rate. The velocity of PAKRP2_NL14 on GMPCPP microtubules was determined to be 59 ± 19 nm s^{-1} (n = 168, Fig. 6 *D*), within 10% of wild-type PAKRP2 (Fig. 2 *E*). Additionally, single-molecule motility assays showed that the neck-shortened motor maintains processivity, but the run length is decreased to 2.0 ± 0.3 μm (n = 168, Fig. 6 *E*), which is 45% less than wild-type (Video S6). The deleted region of the neck linker has a neutral charge, making it unlikely that the reduction in run length is due to weaker electrostatic interactions between the motor domain and the microtubule (67). Therefore, unlike in other kinesins in which longer neck linkers reduce interhead coordination, leading to decreased processivity, the long neck linker of PAKRP2 enhances its processivity.

DISCUSSION

In this study, we revealed that PAKRP2 exhibits processive plus-end-directed motility on single microtubules as individual homodimers. To our knowledge, PARKP2 is the first orphan kinesin motor known to demonstrate processive motility (16–19). Our finding is consistent with the putative role of PAKRP2 in vivo as a vesicle transport kinesin (12). PAKRP2 has a divergent nucleotide-binding motif (12) and hydrolyzes ATP more than 10-fold slower than dimeric kinesin-1 (68,69). It also contains a 32-residue neck linker, which is much longer than most members of the kinesin superfamily (26). Despite these variations in structural features that are integral to motility (43,70), PAKRP2 is more processive than kinesin-1, and it achieves this processivity via a noncanonical stepping mechanism that pairs a long neck linker with a slow ATP hydrolysis cycle. These structural and biochemical features result in a mechanochemical cycle that involves an extended diffusive search of the tethered head for its next binding site and frequent lateral stepping.

In the canonical kinesin motility cycle, ATP turnover is tightly coupled to its forward stepping activity (24,25,66). This coupling is thought to be facilitated by conformational changes in the neck linker, which transmits tension between the two heads to propel the trailing head forward to the next binding site upon ATP hydrolysis (50,51). Evidence for this tension-based mechanism can be seen in the uncoupling of the heads in kinesin-1 with neck linker insertions, which in some cases causes the ATP turnover rate to become much higher than the forward stepping rate (49,51) and in some cases causes the stepping rate to become slower relative to the wild type (43,49). Our study confirms this behavior in

kinesin-1 because the ATP hydrolysis rate of Kin1_NLswap is much higher than the predicted stepping rate (Fig. S6). In contrast, PAKRP2 maintains tight mechanochemical coupling despite having a long neck linker (Fig. 5 *E*), suggesting that the mechanism for motor coupling differs from other kinesins. Consistent with this notion, shortening the PAKRP2 neck linker had no effect on the stepping rate but decreased the run length (Fig. 6, *D* and *E*). These results suggest that the PAKRP2 motor domain and long neck linker have coevolved to achieve tight mechanochemical coupling through an alternative mechanism than the one that has been determined for kinesin-1.

High-resolution particle tracking of PAKRP2 revealed tail displacements of 5.0 nm (Fig. 4 *G*), which is considerably smaller than the 8.2-nm tubulin periodicity, and motor domain displacements of 7.6 nm (Fig. 5 *C*), which is considerably smaller than the 16.4-nm periodicity expected from a classical hand-over-hand mechanism (49,51,62). How does PAKRP2 achieve such unique step sizes? One possibility is that PAKRP2 uses an inchworm-like stepping model, whereby its two motor domains walk on adjacent protofilaments as has been observed for cytoplasmic dynein (34,71). It is worth emphasizing that this type of inchworm stepping differs from the original inchworm model (63,64) in that it involves two catalytically active motor domains and thus consumes two ATP molecules for every single 8.2-nm step. In dynein, this inchworm-like stepping is facilitated by the flexibility between the two heads (72), making it a plausible mode of motion for kinesins with long neck linkers. Our gold particle tracking data do not rule out the possibility that the two PAKRP2 motor domains step on adjacent protofilaments. However, our ATPase data, which show that PAKRP2 burns one ATP molecule per 8.2-nm step, do rule out inchworm stepping as an explanation for the unusual step sizes seen in PAKRP2 (Fig. 5 *E*).

An alternative possibility, which is consistent with the ATPase data, is that the small step sizes observed in PAKRP2 arise from the detection of an intermediate step (or substep) of the tethered motor head before it reaches the next binding site. A 2015 study on kinesin-1 labeled on one motor domain at saturating ATP observed 8.2-nm substeps that were attributed to a transient one-head-bound state after ATP binding and preceding ATP hydrolysis (32). In this study, detection of these intermediate states by particle tracking could be facilitated by the slow stepping rate of PAKRP2, which is ~20-fold slower than kinesin-1. Step sizes smaller than 16.4 nm have been previously observed in kinesin-1 mutants with long neck linkers, but they were not attributed to substeps (49). In support of a transient one-head-bound state, a recent study demonstrated that the duration of the one-head-bound state can be increased by increasing the neck linker length in kinesin-1 and kinesin-2 motors, an effect that may result from an increase in the area of a diffusional search taken by the tethered head before binding (27). Taken together, the PAKRP2 data are most consistent with a substep model, though the exact mechanism of this substep may be different than that of kinesin-1. In canonical processive steppers, such as kinesin-1 and kinesin-2, extending the one-head-bound state duration leads to a higher probability that the bound head detaches before the tethered head binds and, consequently, causes a reduction in processivity of the motor (27). In contrast, the intermediate state in PAKRP2 is more than 10 times longer than the transient state (<10 ms) in kinesin-1 (32), and shortening the neck linker of PAKRP2, which presumably decreases the one-head-bound state duration, does not increase the processivity (Fig. 6 *E*).

Another example of a kinesin with an unusually long neck linker is Zen4, a member of the kinesin-6 family that plays a role in microtubule organization during cytokinesis (73). The neck linker of Zen4 is 75 residues long and includes a binding site for GTPase-activating proteins (74) but does not prevent the motor from processively stepping along microtubules (75). The crystal structure of the Zen4 motor domain in a nucleotide-free state revealed that the initial segment of the neck linker docked in a backward conformation; this conformation is thought to relieve interhead tension and allow for more stability in the two-head-bound state (75). Zen4 functions primarily in cross-linking microtubules, so the long neck linker, coupled with backward docking in the two-head-bound state, could potentially allow both motor heads to remain bound for long periods of time. However, despite both motors having long neck linkers, PAKRP2 does not contain the "arginine gate" that facilitates the backward docking of the neck linker, and it is not clear how the stabilization of the two-head-bound state would benefit a transport motor. Thus, parallels that can be drawn between Zen4 and PAKRP2 are limited.

Although long neck linkers are mainly viewed as a disadvantage for processivity (22,26,43,49), studies have shown that they are an advantage for obstacle avoidance. Kinesin-2, which contains a 17-residue neck linker, has been shown to occasionally step laterally to adjacent protofilaments (56) and to be less affected than kinesin-1 by the addition of roadblocks, such as the τ protein or rigor kinesin-1 motors on the microtubule track (76). These studies propose that a long neck linker makes kinesin-2 sufficiently flexible to step to many of the adjacent binding sites to circumvent obstacles and therefore less likely to dissociate from the microtubule. This idea is further supported by clear lateral steps in kinesin-1 mutants with extended neck linkers (49). In the cell, microtubules are decorated with microtubule-associated proteins that could potentially block the paths of processive motors (77–80), and so this obstacle avoidance could provide a selective advantage in maximizing transport. Given that PAKRP2 is thought to transport materials on the phragmoplast microtubules, it seems likely that it encounters microtubule-associated proteins, and side stepping would be a useful feature. As a final point, consecutive side steps have also been observed for kinesin-8, a processive, microtubule-length

regulator with a 17-residue neck linker (31,81–84). Thus, frequent side stepping is a possibility for processive kinesins even though it is rarely observed in kinesin families responsible for transport (56,57).

Based on these results, we propose that PAKRP2 steps via a hand-over-hand mechanism that includes a transient intermediate state, thus broadly resembling the canonical stepping mechanism laid out for kinesin-1 and other processive N-terminal kinesins (28,58,62,64). However, unlike the canonical mechanism, the stepping behavior of PAKRP2 includes a prolonged one-head-bound state that does not compromise its processivity, many lateral steps, and tight coupling of ATP hydrolysis to forward stepping despite the motor having an extended neck linker domain. Further single-molecule work is needed to precisely determine how PAKRP2 achieves processive stepping and tight mechanochemical coupling, despite having an extended neck linker. It is also not known how the long neck linker might impact the ability of PAKRP2 to generate sustained forces. From a biological perspective, there is still no direct evidence that PAKRP2 can associate with vesicle membranes, and it is not clear whether intracellular transport by PAKRP2 generally results from a small population of motors or a large ensemble of motors attached to the cargo. Overall, these results add to the developing model of kinesin stepping, wherein each motor steps in a way that is optimized for its structure and role in the cell.

SUPPORTING MATERIAL

Supporting Material can be found online at https://doi.org/10.1016/j.bpj.2019.02.019.

AUTHOR CONTRIBUTIONS

W.Q. conceived and supervised the study. A.M.G. and P.W. performed all experiments. C.L. provided reagents. K.J.M. built the microscope used for high-resolution tracking and assisted with experiments and analysis. A.M.G., W.O.H., and W.Q. wrote the manuscript with input from all authors.

ACKNOWLEDGMENTS

This project was supported through grants from the National Science Foundation to W.Q. (1616462) and the National Institutes of Health to W.O.H. (R01GM076476). P.W. was supported by a visiting student scholarship from the China Scholarship Council (grant number 201608410124) and through grants from the National Science Foundation Committee of China (project numbers U1604129 and 21173068 to L.G.). K.J.M. was supported by a fellowship from the National Cancer Institute (F99CA223018).

REFERENCES

1. Wordeman, L. 2010. How kinesin motor proteins drive mitotic spindle function: lessons from molecular assays. *Semin. Cell Dev. Biol.* 21:260–268.
2. Fukuda, Y., A. Luchniak, …, M. L. Gupta, Jr. 2014. Spatial control of microtubule length and lifetime by opposing stabilizing and destabilizing functions of kinesin-8. *Curr. Biol.* 24:1826–1835.
3. Ferenz, N. P., A. Gable, and P. Wadsworth. 2010. Mitotic functions of kinesin-5. *Semin. Cell Dev. Biol.* 21:255–259.
4. She, Z. Y., and W. X. Yang. 2017. Molecular mechanisms of kinesin-14 motors in spindle assembly and chromosome segregation. *J. Cell Sci.* 130:2097–2110.
5. Goshima, G., and R. D. Vale. 2003. The roles of microtubule-based motor proteins in mitosis: comprehensive RNAi analysis in the Drosophila S2 cell line. *J. Cell Biol.* 162:1003–1016.
6. Hirokawa, N., and Y. Noda. 2008. Intracellular transport and kinesin superfamily proteins, KIFs: structure, function, and dynamics. *Physiol. Rev.* 88:1089–1118.
7. Hirokawa, N., Y. Noda, …, S. Niwa. 2009. Kinesin superfamily motor proteins and intracellular transport. *Nat. Rev. Mol. Cell Biol.* 10:682–696.
8. Encalada, S. E., L. Szpankowski, …, L. S. Goldstein. 2011. Stable kinesin and dynein assemblies drive the axonal transport of mammalian prion protein vesicles. *Cell.* 144:551–565.
9. Maday, S., A. E. Twelvetrees, …, E. L. Holzbaur. 2014. Axonal transport: cargo-specific mechanisms of motility and regulation. *Neuron.* 84:292–309.
10. de Keijzer, J., B. M. Mulder, and M. E. Janson. 2014. Microtubule networks for plant cell division. *Syst. Synth. Biol.* 8:187–194.
11. Bajer, A., and R. D. Allen. 1966. Role of phragmoplast filaments in cell-plate formation. *J. Cell Sci.* 1:455–462.
12. Lee, Y. R., H. M. Giang, and B. Liu. 2001. A novel plant kinesin-related protein specifically associates with the phragmoplast organelles. *Plant Cell.* 13:2427–2439.
13. Lawrence, C. J., R. K. Dawe, …, L. Wordeman. 2004. A standardized kinesin nomenclature. *J. Cell Biol.* 167:19–22.
14. Shen, Z., A. R. Collatos, …, L. Vidali. 2012. Phylogenetic analysis of the kinesin superfamily from physcomitrella. *Front. Plant Sci.* 3:230.
15. Chesarone-Cataldo, M., C. Guérin, …, B. L. Goode. 2011. The myosin passenger protein Smy1 controls actin cable structure and dynamics by acting as a formin damper. *Dev. Cell.* 21:217–230.
16. Sisson, J. C., K. S. Ho, …, M. P. Scott. 1997. Costal2, a novel kinesin-related protein in the Hedgehog signaling pathway. *Cell.* 90:235–245.
17. Hu, H., L. Hu, …, Z. Li. 2012. An orphan kinesin in trypanosomes cooperates with a kinetoplastid-specific kinesin to maintain cell morphology by regulating subpellicular microtubules. *J. Cell Sci.* 125:4126–4136.
18. Hiwatashi, Y., M. Obara, …, M. Hasebe. 2008. Kinesins are indispensable for interdigitation of phragmoplast microtubules in the moss Physcomitrella patens. *Plant Cell.* 20:3094–3106.
19. Lillie, S. H., and S. S. Brown. 1998. Smy1p, a kinesin-related protein that does not require microtubules. *J. Cell Biol.* 140:873–883.
20. Jonsson, E., M. Yamada, …, G. Goshima. 2015. Clustering of a kinesin-14 motor enables processive retrograde microtubule-based transport in plants. *Nat. Plants.* 1:15087.
21. Vale, R. D., T. Funatsu, …, T. Yanagida. 1996. Direct observation of single kinesin molecules moving along microtubules. *Nature.* 380:451–453.
22. Shastry, S., and W. O. Hancock. 2011. Interhead tension determines processivity across diverse N-terminal kinesins. *Proc. Natl. Acad. Sci. USA.* 108:16253–16258.
23. Soppina, V., S. R. Norris, …, K. J. Verhey. 2014. Dimerization of mammalian kinesin-3 motors results in superprocessive motion. *Proc. Natl. Acad. Sci. USA.* 111:5562–5567.
24. Schnitzer, M. J., and S. M. Block. 1997. Kinesin hydrolyses one ATP per 8-nm step. *Nature.* 388:386–390.
25. Hua, W., E. C. Young, …, J. Gelles. 1997. Coupling of kinesin steps to ATP hydrolysis. *Nature.* 388:390–393.

26. Düselder, A., C. Thiede, …, S. Lakämper. 2012. Neck-linker length dependence of processive kinesin-5 motility. *J. Mol. Biol.* 423:159–168.

27. Mickolajczyk, K. J., and W. O. Hancock. 2017. Kinesin processivity is determined by a kinetic race from a vulnerable one-head-bound state. *Biophys. J.* 112:2615–2623.

28. Hancock, W. O. 2016. The kinesin-1 chemomechanical cycle: stepping toward a consensus. *Biophys. J.* 110:1216–1225.

29. Furuta, K., A. Furuta, …, H. Kojima. 2013. Measuring collective transport by defined numbers of processive and nonprocessive kinesin motors. *Proc. Natl. Acad. Sci. USA.* 110:501–506.

30. Popchock, A. R., K. F. Tseng, …, W. Qiu. 2017. The mitotic kinesin-14 KlpA contains a context-dependent directionality switch. *Nat. Commun.* 8:13999.

31. Mayr, M. I., M. Storch, …, T. U. Mayer. 2011. A non-motor microtubule binding site is essential for the high processivity and mitotic function of kinesin-8 Kif18A. *PLoS One.* 6:e27471.

32. Mickolajczyk, K. J., N. C. Deffenbaugh, …, W. O. Hancock. 2015. Kinetics of nucleotide-dependent structural transitions in the kinesin-1 hydrolysis cycle. *Proc. Natl. Acad. Sci. USA.* 112:E7186–E7193.

33. Bieling, P., L. Laan, …, T. Surrey. 2007. Reconstitution of a microtubule plus-end tracking system in vitro. *Nature.* 450:1100–1105.

34. Qiu, W., N. D. Derr, …, S. L. Reck-Peterson. 2012. Dynein achieves processive motion using both stochastic and coordinated stepping. *Nat. Struct. Mol. Biol.* 19:193–200.

35. Thompson, A. R., G. J. Hoeprich, and C. L. Berger. 2013. Single-molecule motility: statistical analysis and the effects of track length on quantification of processive motion. *Biophys. J.* 104:2651–2661.

36. Chen, G. Y., K. J. Mickolajczyk, and W. O. Hancock. 2016. The kinesin-5 chemomechanical cycle is dominated by a two-heads-bound state. *J. Biol. Chem.* 291:20283–20294.

37. Feng, Q., K. J. Mickolajczyk, …, W. O. Hancock. 2018. Motor reattachment kinetics play a dominant role in multimotor-driven cargo transport. *Biophys. J.* 114:400–409.

38. Ruhnow, F., D. Zwicker, and S. Diez. 2011. Tracking single particles and elongated filaments with nanometer precision. *Biophys. J.* 100:2820–2828.

39. Chen, Y., N. C. Deffenbaugh, …, W. O. Hancock. 2014. Molecular counting by photobleaching in protein complexes with many subunits: best practices and application to the cellulose synthesis complex. *Mol. Biol. Cell.* 25:3630–3642.

40. Huang, T. G., and D. D. Hackney. 1994. Drosophila kinesin minimal motor domain expressed in Escherichia coli. Purification and kinetic characterization. *J. Biol. Chem.* 269:16493–16501.

41. Chen, G. Y., D. F. Arginteanu, and W. O. Hancock. 2015. Processivity of the kinesin-2 KIF3A results from rear head gating and not front head gating. *J. Biol. Chem.* 290:10274–10294.

42. Case, R. B., S. Rice, …, R. D. Vale. 2000. Role of the kinesin neck linker and catalytic core in microtubule-based motility. *Curr. Biol.* 10:157–160.

43. Shastry, S., and W. O. Hancock. 2010. Neck linker length determines the degree of processivity in kinesin-1 and kinesin-2 motors. *Curr. Biol.* 20:939–943.

44. Andreasson, J. O., B. Milic, …, S. M. Block. 2015. Examining kinesin processivity within a general gating framework. *eLife.* 4:e07403.

45. Rice, S., A. W. Lin, …, R. D. Vale. 1999. A structural change in the kinesin motor protein that drives motility. *Nature.* 402:778–784.

46. Wickstead, B., and K. Gull. 2006. A "holistic" kinesin phylogeny reveals new kinesin families and predicts protein functions. *Mol. Biol. Cell.* 17:1734–1743.

47. Lupas, A., M. Van Dyke, and J. Stock. 1991. Predicting coiled coils from protein sequences. *Science.* 252:1162–1164.

48. Delorenzi, M., and T. Speed. 2002. An HMM model for coiled-coil domains and a comparison with PSSM-based predictions. *Bioinformatics.* 18:617–625.

49. Yildiz, A., M. Tomishige, …, R. D. Vale. 2008. Intramolecular strain coordinates kinesin stepping behavior along microtubules. *Cell.* 134:1030–1041.

50. Hackney, D. D., M. F. Stock, …, R. A. Patterson. 2003. Modulation of kinesin half-site ADP release and kinetic processivity by a spacer between the head groups. *Biochemistry.* 42:12011–12018.

51. Clancy, B. E., W. M. Behnke-Parks, …, S. M. Block. 2011. A universal pathway for kinesin stepping. *Nat. Struct. Mol. Biol.* 18:1020–1027.

52. Tseng, K. F., P. Wang, …, W. Qiu. 2018. The preprophase band-associated kinesin-14 OsKCH2 is a processive minus-end-directed microtubule motor. *Nat. Commun.* 9:1067.

53. Yajima, H., T. Ogura, …, N. Hirokawa. 2012. Conformational changes in tubulin in GMPCPP and GDP-taxol microtubules observed by cryoelectron microscopy. *J. Cell Biol.* 198:315–322.

54. McVicker, D. P., L. R. Chrin, and C. L. Berger. 2011. The nucleotide-binding state of microtubules modulates kinesin processivity and the ability of Tau to inhibit kinesin-mediated transport. *J. Biol. Chem.* 286:42873–42880.

55. Vale, R. D., C. M. Coppin, …, R. A. Milligan. 1994. Tubulin GTP hydrolysis influences the structure, mechanical properties, and kinesin-driven transport of microtubules. *J. Biol. Chem.* 269:23769–23775.

56. Hoeprich, G. J., K. J. Mickolajczyk, …, C. L. Berger. 2017. The axonal transport motor kinesin-2 navigates microtubule obstacles via protofilament switching. *Traffic.* 18:304–314.

57. Schneider, R., T. Korten, …, S. Diez. 2015. Kinesin-1 motors can circumvent permanent roadblocks by side-shifting to neighboring protofilaments. *Biophys. J.* 108:2249–2257.

58. Yildiz, A., and P. R. Selvin. 2005. Fluorescence imaging with one nanometer accuracy: application to molecular motors. *Acc. Chem. Res.* 38:574–582.

59. Svoboda, K., C. F. Schmidt, …, S. M. Block. 1993. Direct observation of kinesin stepping by optical trapping interferometry. *Nature.* 365:721–727.

60. Amos, L., and A. Klug. 1974. Arrangement of subunits in flagellar microtubules. *J. Cell Sci.* 14:523–549.

61. Kojima, H., E. Muto, …, T. Yanagida. 1997. Mechanics of single kinesin molecules measured by optical trapping nanometry. *Biophys. J.* 73:2012–2022.

62. Yildiz, A., M. Tomishige, …, P. R. Selvin. 2004. Kinesin walks hand-over-hand. *Science.* 303:676–678.

63. Hua, W., J. Chung, and J. Gelles. 2002. Distinguishing inchworm and hand-over-hand processive kinesin movement by neck rotation measurements. *Science.* 295:844–848.

64. Asbury, C. L., A. N. Fehr, and S. M. Block. 2003. Kinesin moves by an asymmetric hand-over-hand mechanism. *Science.* 302:2130–2134.

65. Stepp, W. L., G. Merck, …, Z. Ökten. 2017. Kinesin-2 motors adapt their stepping behavior for processive transport on axonemes and microtubules. *EMBO Rep.* 18:1947–1956.

66. Coy, D. L., M. Wagenbach, and J. Howard. 1999. Kinesin takes one 8-nm step for each ATP that it hydrolyzes. *J. Biol. Chem.* 274:3667–3671.

67. Thorn, K. S., J. A. Ubersax, and R. D. Vale. 2000. Engineering the processive run length of the kinesin motor. *J. Cell Biol.* 151:1093–1100.

68. Jiang, W., M. F. Stock, …, D. D. Hackney. 1997. Influence of the kinesin neck domain on dimerization and ATPase kinetics. *J. Biol. Chem.* 272:7626–7632.

69. Woehlke, G., A. K. Ruby, …, R. D. Vale. 1997. Microtubule interaction site of the kinesin motor. *Cell.* 90:207–216.

70. Cross, R. A. 2016. Review: mechanochemistry of the kinesin-1 ATPase. *Biopolymers.* 105:476–482.

71. DeWitt, M. A., A. Y. Chang, …, A. Yildiz. 2012. Cytoplasmic dynein moves through uncoordinated stepping of the AAA+ ring domains. *Science.* 335:221–225.

72. Bhabha, G., G. T. Johnson, …, R. D. Vale. 2016. How dynein moves along microtubules. *Trends Biochem. Sci.* 41:94–105.

73. White, E. A., and M. Glotzer. 2012. Centralspindlin: at the heart of cytokinesis. *Cytoskeleton (Hoboken).* 69:882–892.

74. Mishima, M., S. Kaitna, and M. Glotzer. 2002. Central spindle assembly and cytokinesis require a kinesin-like protein/RhoGAP complex with microtubule bundling activity. *Dev. Cell.* 2:41–54.

75. Guan, R., L. Zhang, …, Z. Chen. 2017. Crystal structure of Zen4 in the apo state reveals a missing conformation of kinesin. *Nat. Commun.* 8:14951.

76. Hoeprich, G. J., A. R. Thompson, …, C. L. Berger. 2014. Kinesin's neck-linker determines its ability to navigate obstacles on the microtubule surface. *Biophys. J.* 106:1691–1700.

77. Kinoshita, K., B. Habermann, and A. A. Hyman. 2002. XMAP215: a key component of the dynamic microtubule cytoskeleton. *Trends Cell Biol.* 12:267–273.

78. Drewes, G., A. Ebneth, and E. M. Mandelkow. 1998. MAPs, MARKs and microtubule dynamics. *Trends Biochem. Sci.* 23:307–311.

79. Mandelkow, E., and E. M. Mandelkow. 1995. Microtubules and microtubule-associated proteins. *Curr. Opin. Cell Biol.* 7:72–81.

80. Permana, S., S. Hisanaga, …, T. J. Itoh. 2005. Truncation of the projection domain of MAP4 (microtubule-associated protein 4) leads to attenuation of microtubule dynamic instability. *Cell Struct. Funct.* 29:147–157.

81. Bormuth, V., B. Nitzsche, …, S. Diez. 2012. The highly processive kinesin-8, Kip3, switches microtubule protofilaments with a bias toward the left. *Biophys. J.* 103:L4–L6.

82. Su, X., W. Qiu, …, D. Pellman. 2011. Mechanisms underlying the dual-mode regulation of microtubule dynamics by Kip3/kinesin-8. *Mol. Cell.* 43:751–763.

83. Mitra, A., F. Ruhnow, …, S. Diez. 2018. Directionally biased sidestepping of Kip3/kinesin-8 is regulated by ATP waiting time and motor-microtubule interaction strength. *Proc. Natl. Acad. Sci. USA.* 115:E7950–E7959.

84. Varga, V., J. Helenius, …, J. Howard. 2006. Yeast kinesin-8 depolymerizes microtubules in a length-dependent manner. *Nat. Cell Biol.* 8:957–962.